Photosensitive Salt Distribution in Polymer Films Studied by ^{19}F Multiple-Quantum NMR

Bruce E. Scruggs and Karen K. Gleason*

Department of Chemical Engineering, Massachusetts Institute of Technology, Cambridge, Massachusetts 02139

Received September 11, 1991

ABSTRACT: In this work, the dispersion of triphenylsulfonium metal–fluoride salts in polymer films modeling chemically amplified resist systems has been characterized by solid-state ^{19}F multiple-quantum nuclear magnetic resonance (MQ-NMR). Previously, this technique has been used to characterize ^{1}H distributions on a length scale of ~20 Å in various materials. In agreement with differential scanning calorimetry, metal–fluoride salts were shown to be immiscible with the nonpolar polymers poly(*n*-butyl methacrylate) (PnBMA) and poly(isobutyl methacrylate) (PiBMA), with no indication of individual salt molecules solubilized within the polymer matrix. Metal–fluoride salts in poly(methyl methacrylate) (PMMA) were observed to be dispersed on a molecular scale even at a salt loading of 20% w/w. Although observed by electron microscopy, evidence of larger aggregates is absent in the MQ-NMR data of the salt/PMMA films, indicating that these aggregates represent a small fraction of the total salt in these films. In addition, unlike electron microscopy, MQ-NMR is nondestructive with respect to the photosensitive salt and polymers comprising resist systems.

Introduction

Chemical amplification resists are being developed to provide an advanced lithographic system demonstrating high sensitivity to <350-nm-wave-length radiation and the capability to resolve submicron features. These advanced resists are typically mixtures of a polymer and an acid-generating photosensitive compound. Upon irradiation, the photosensitive compound is converted to a strong acid, which during a postbake step, catalytically induces reactions which alter the solubility of the polymer matrix.[1-4]

In an effort to understand the fundamental factors which influence catalytic resist chemistry, recent work has characterized the conversion of a triphenylsulfonium salt to acid for a homologous series of methacrylate polymer matrices.[5] As the length of the alkyl side chain and, hence, the polarity of the polymeric matrix is varied, the distribution of salt within the polymer varies. A strong correlation has been observed between the conversion of a triphenylsulfonium salt to its corresponding Brönsted acid and the degree of salt dispersion within the polymeric matrix. A primary radical pathway for the acid conversion of the triphenylsulfonium salt involves hydrogen abstraction from the polymer. Hence, intimate mixing of the salt in the polymeric matrix should be expected to promote the acid conversion reaction.[6] Intimate mixing of the salt in the matrix is also desired to maximize the total number of catalytic events which can occur, since the diffusion length of the acid during the postbake step is only on the order of 50 Å.[7]

Previously, the extent of mixing of photosensitive sulfonium salt/polymer blends has been characterized by differential scanning calorimetry (DSC) and scanning electron microscopy (SEM).[5] The triphenylsulfonium salt/polymer interaction is an energetically weak interaction which serves to enhance the motion of polymer chains plasticizing the polymeric matrix and lowering the polymer glass transition temperature, T_g. Stronger interactions which involve electron transfer between bonding orbitals, such as alkali metal–oxygen complexation in alkali-metal salt/poly(ethylene oxide) blends, increase the polymer T_g by inhibiting motion of the polymer chains.[8] The depression of the T_g with salt concentration and the manifestation of a salt melting peak measured by DSC were both used to describe the blending of the sulfonium salt/polymer mixtures. SEM of film fracture surfaces produced at liquid-nitrogen temperatures has directly observed salt aggregates in these salt/polymer films on a length scale as small as 700 Å.

Although not previously reported for sulfonium salts, infrared (IR) spectroscopy has been used to characterize the dispersion of inorganic salts in polymeric matrices. Strong complexation interactions involving alkali-metal cations and a functional group of the polymer, such as a carbonyl, have been observed as a shift in the IR frequency of the polymer absorption.[9,10] However, it is unlikely that the weak salt/polymer plasticizer interaction involves the type of electron transfer between interacting chemical functional groups that would lead to a shift in the IR band of the polymer carbonyl group or various metal–fluoride salt bands.

The main focus of this work is to apply ^{19}F multiple-quantum (MQ) nuclear magnetic resonance (NMR) spectroscopy to characterize the dispersion in polymer films of acid-generating salts composed of a photosensitive organic cation and a metal–fluoride anion. MQ-NMR spectroscopy has proven useful in studying the distribution of nuclei in amorphous materials on a length scale on the order of 10 Å. It has previously been used to elucidate the distribution of hydrogen in amorphous silicon[11] and silicon carbide[12] and adsorption of organic molecules containing hydrogen in zeolites[13,14] and on catalytic surfaces.[15] While these MQ-NMR studies of atomic-scale clustering in solids have used ^{1}H as a probe nucleus, ^{19}F is also an attractive candidate. Like ^{1}H, ^{19}F is a spin-$^{1}/_{2}$ nuclei with a natural abundance of 100%, making isotopic enrichment unnecessary. The magnetic moment of ^{19}F is 94% that of ^{1}H, providing high NMR sensitivity and strong homonuclear ^{19}F–^{19}F dipole couplings, which are responsible for the development of MQ coherences. In addition, the ^{19}F MQ-NMR signal arises only from the photoactive metal–fluoride salt, for which distribution information is sought, while no background signal arises from the polymer matrix, which comprises the majority of the sample. Finally, NMR requires only low-energy radio-frequency radiation, which is nondestructive to the photosensitive compounds used

* Author to whom correspondence should be addressed.

0024-9297/92/2225-1864$03.00/0

in chemically amplified resists, unlike the higher energy radiation employed by X-ray diffraction and transmission electron microscopy (TEM).

Theory

MQ-NMR is a two-dimensional experiment involving both a preparation and a mixing period.[16-19] The preparation period is composed of an integer number of repeating eight $\pi/2$-pulse subcycles. During the preparation period, multiple-spin transitions known as MQ coherences are created as individual nuclei become correlated through their dipole couplings. Coherences, having order n, indicate correlation between two states which differ in the z-component of angular momentum by n units. Thus, a least n dipole-coupled spin-$^1/_2$ nuclei are required to create an n-quantum coherence. As longer preparation times, τ, are achieved through increased repetition of the eight-pulse subcycle, larger groups of spins become correlated.

The particular eight-pulse subcycle used[18] excites only even-order MQ coherences, improving the signal to noise ratio of the spectrum. The various n-order coherences can be separated by shifting the phase, ϕ, of the preparation period from 0° to (360° − $\Delta\phi$) by increments of $\Delta\phi$ degrees while fixing the mixing period phase, since the signal from each order involves a complex term, $\exp(in\Delta\phi)$. Fourier transformation with respect to ϕ yields an MQ spectrum containing the intensities of each order where $|n| \leq \pi/\Delta\phi$.

The mixing period is identical to the preparation period at $\phi = 90°$. This portion of the experiment results in time reversal,[11] causing the signal intensity of each MQ order to add constructively, further enhancing the signal to noise ratio. The mixing period also serves to convert unobservable MQ coherences into observable magnetization. After a 1-ms delay to allow for decay of signal transients, a $\pi/2$ detection pulse is applied in order to observe the stored MQ magnetization. Since only the signal intensity as a function of ϕ is required, spin-locking with periodic sampling was employed to further enhance the signal to noise ratio.[18]

At a given preparation time, τ, the effective number of correlated nuclei, $N(\tau)$, has previously been described by a simple statistical model in which the total intensity of an n-order coherence, $I(n,\tau)$ is directly proportional to the number of ways of achieving that coherence within the 2^N energy levels of the N dipole-coupled spins.[17] Assuming all MQ coherences occur with equal probability at all τ, the intensities of the nonzero MQ coherences can be described by a Gaussian distribution

$$I(n,\tau) \propto \exp[-n^2/N(\tau)] \quad (1)$$

when $N(\tau) \geq 6$. Although it is not valid for all spin systems, the statistical model has yielded consistent results in strongly dipole-coupled solids.[17,21]

The growth rate of $N(\tau)$ with the preparation time depends on both the magnitude and the number of dipole couplings within the sample. For a pair of spins, the strength of the dipole coupling depends on the inverse cube of the internuclear separation. Stronger dipole couplings result in MQ coherence development at short τ values, producing a fast $N(\tau)$ growth rate. In order to develop high-order MQ coherences involving larger groups of correlated spins, longer preparation times are required.[17] The induction time required to generate an n-quantum coherence has been related to the square root of the second-moment of the ^{19}F–^{19}F dipolar coupling in fluorine-containing salts.[21] Thus, longer induction periods are indicative of larger interanion spacings, which reflect the local salt distribution.

A finite cluster of dipole-coupled spins will be limited in the extent of MQ coherences which can be achieved. The cluster size is determined by the value at which $N(\tau)$ saturates as τ is increased. The liquid crystal p-hexyl-p'-cyanobiphenyl, $C_{19}H_{21}N$, is an example of such a finite cluster.[17] In this molecule, anisotropic rotation and translation serve to destroy intermolecule dipole couplings, while intramolecular dipole couplings maintain nonzero values. In agreement with the statistical model (eq 1) the observed values of $I(n,\tau)$ follows a Gaussian envelope for $n > 0$. In addition, the value of $N(\tau)$ calculated saturates at $N = 20 \pm 1$, as expected from the structural formula. Thus, MQ-NMR can give quantitative information on the number of nuclei in a given cluster, allowing MQ-NMR to be used as a spin-counting technique.

In a strongly dipole-coupled spin system which is much larger than the 10–20-Å length scale of a typical MQ-NMR experiment, the effective number of coupled spins does not saturate but rather grows continuously with τ, reflecting the "infinite" nature of the dipole-coupling network. Thus, in the absence of relaxation, the parameter $N(\tau)$ will grow without bound as τ is incremented. It should be noted, however, that since the effective number of interacting spins is an ill-defined concept in a strongly dipolar-coupled solid, $N(\tau)$ should be regarded as a parameter which reflects both the structure of and molecular reorientations within the solid.[17]

Table I
Solution-Cast Photosensitive Salt/Polymer Films Characterized by Solid-State ^{19}F MQ-NMR

salt/polymer film[a]	M_w	polydispersity
98% Ph_3SAsF_6		
1% Ph_3SAsF_6/PnBMA	320 000	4.4
1% Ph_3SAsF_6/PiBMA	300 000	2.1
1% Ph_3SAsF_6/PMMA	93 000	2.0
1% Ph_3SAsF_6/PMMA	420 000	4.1
10% Ph_3SSbF_6/PnBMA[b]	102 000[c]	2.2[c]
10% Ph_3SSbF_6/PMMA[b]	70 500[c]	2.0[c]
20% Ph_3SSbF_6/PMMA[b]	70 500[c]	2.0[c]

[a] % w/w salt/polymer. [b] Films provided by Dr. Robert Allen (IBM, Almaden Research Center, San Jose, CA). [c] From ref 5.

Experimental Section

Materials. Secondary standard polymers, poly(methyl methacrylate) (PMMA), poly(n-butyl methacrylate) (PnBMA), and poly(isobutyl methacrylate) (PiBMA), were used as obtained from Aldrich. These polymers were chosen since previous work[5] has indicated that triphenylsulfonium hexafluoroantimonate, Ph_3SSbF_6, is largely dispersed within the PMMA matrix while being highly aggregated in the PnBMA matrix. The solubility of sulfonium metal–fluoride salts in a polymeric matrix is a strong function of the matrix polarity. In comparison to PnBMA and PiBMA, PMMA forms a highly polar matrix. Triphenylsulfonium hexafluoroarsenate, Ph_3SAsF_6, 98% with 2% NaF, was used as obtained from Johnson Matthey/Alpha.

Sample Preparation. The salt/polymer mixtures examined in this work are shown in Table I. Films prepared in this laboratory were solution cast from 6% w/w (polymer/solvent) tetrahydrofuran solutions doped with 1% w/w Ph_3SAsF_6/polymer. In order to remove residual solvents, films were allowed to air dry for ~48 h followed by a vacuum anneal at 130 °C for 1 h. Samples were then heated at 70 °C for 48 h at essentially atmospheric pressure and allowed to slowly cool to room temperature. Preparation of the remaining films in Table I, obtained from Dr. Robert Allen of IBM's Almaden Research Center, has been described elsewhere.[5]

Physical Characterization. MQ-NMR spectroscopy was performed on a home-built NMR spectrometer with a 300-MHz ^1H Larmor frequency. Phase shifting of the preparation period

pulses with respect to the mixing period pulses was achieved with a 270-MHz Sciteq digital synthesizer with 8-bit phase-shifting capability. The incremental preparation phase shift, $\Delta\phi$, was set at 5.6°, allowing detection of coherences with $|n| \leq 16$. All MQ spectra were taken at 200 K, unless otherwise noted, in order to enhance the signal to noise ratio and shorten spin–lattice relaxation time constants. The NMR samples contained anywhere from 4 to 20 mg of Ph_3SSbF_6 or Ph_3SAsF_6 salts.

The length of $\pi/2$ pulses used ranged from 2.5 to 2.8 μs, while the basic MQ pulse sequence cycle time, t_c, was held fixed at 60 μs. A pulsed spin-locking detection sequence of 5 ms in length was used during the detection period for signal enhancement.[18]

Selected samples of Ph_3SSbF_6 in PMMA and PnBMA were further characterized with IR spectroscopy, DSC, and TEM. The IR data were acquired on a Nicolet 800 FT-IR spectrometer using an internal reflectance microsampling accessory. DSC analysis was performed on a Perkin-Elmer DSC-7 at a temperature scanning rate of 10 °C/min. The T_g of a polymer film was taken as the midpoint of the heating inflection. A TopCon 200-kV TEM Model EM-002B microscope was used to examine samples which were coated with ~100 Å of evaporated carbon in order to reduce heating and charging effects.

Results and Discussion

Free Induction Decay NMR. Ideally, the distribution of magnetic nuclei in a sample film could be described by the homonuclear dipolar line width of the Fourier-transformed free-induction-decay (FID) spectrum. For Ph_3SSbF_6 and Ph_3SAsF_6, this line width would represent only intermolecular interactions, since the rapid, isotropic rotation of these anions averages the intramolecular homonuclear ^{19}F–^{19}F dipole couplings to zero.[20,21] In Figure 1, the room-temperature ^{19}F FID spectra of 10% w/w Ph_3SSbF_6 in PMMA and PnBMA are compared. Large-scale (>1-μm) aggregates of salt are expected in nonpolar PnBMA, while salt dispersed on a molecular level is anticipated in the relatively polar PMMA matrix at this salt loading, based on previously reported DSC and SEM analysis.[5] Clearly, the two line shapes of Figure 1a are virtually identical in shape and width, despite the expected differences in salt dispersion. Strong heteronuclear ^1H–^{19}F dipole couplings complicate the dipolar structure of these materials, obscuring the homonuclear dipolar line width. Removal of the ^1H–^{19}F interaction by proton spin decoupling techniques, a difficult experimental task for high-power solid-state NMR spectroscopy, will not necessarily resolve the problem of measuring homonuclear ^{19}F–^{19}F dipole line widths since the SbF_6^- and AsF_6^- anions also display large metal–fluoride scalar or J couplings on the order of one kilohertz.[20,22]

MQ-NMR. Heteronuclear dipole and scalar couplings, which prohibit the use of NMR line shapes to examine acid-generating salt distribution in polymer films, do not affect the correlation of ^{19}F nuclei under the influence of the solid-state multiple-quantum pulse Hamiltonian. Zeroth-order-average Hamiltonian calculations show that the heteronuclear dipolar interaction is averaged to zero by the eight-pulse MQ solid-state sequence.[21] This is also true for heteronuclear J couplings, which have the same mathematical form as heteronuclear dipole couplings. Experimentally, this has been verified in our laboratory through comparison of the $N(\tau)$ growth rates for $NaAsF_6$ and Ph_3SAsF_6.[21] Thus, heteronuclear couplings do not affect the potential of MQ-NMR for examining the distribution of Ph_3SSbF_6 and Ph_3SAsF_6 on a molecular level in protonated polymer films.

As a demonstration of this last assertion, parts b and c of Figure 1 show the MQ spectra at τ = 960 μs for the same two films which gave the identical NMR line shapes shown in Figure 1a. There is a clear difference in the

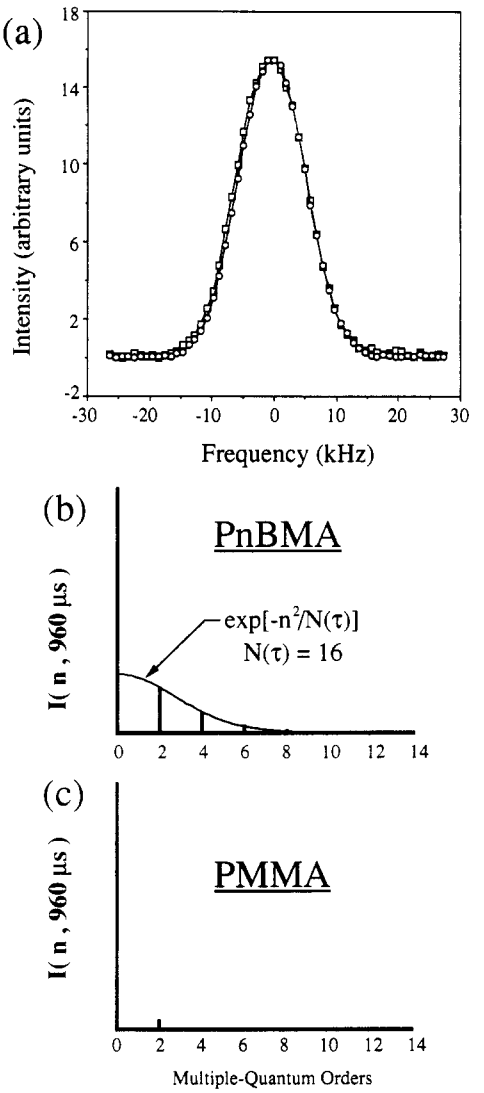

Figure 1. (a) For 10% w/w Ph_3SSbF_6 in two different polymer films, Fourier-transformed free-induction-decay NMR spectra of PnBMA (open squares) and PMMA (open circles) films. The two resonances are indistinguishable within experimental uncertainty. (b) MQ-NMR spectra at τ = 960 μs for the 10% Ph_3SSbF_6/PnBMA film, showing intensities at 2, 4, 6, and 8 orders, which follow a Gaussian distribution (solid line) indicative of 16-correlated ^{19}F (eq 1). (c) In contrast, the 10% Ph_3SSbF_6/PMMA film's spectrum does not contain appreciable 4, 6, or 8-quantum coherences, indicating a lower local ^{19}F density than that in the PnBMA film, even though both films have the same overall 10% salt loading. Thus, the difference in salt distribution between the PnBMA and PMMA films with 10% salt is observed by MQ-NMR, although not by the traditional NMR experiment.

nonzero MQ coherence intensities between the PnBMA and PMMA films even though both have the same 10% salt loading. The Gaussian fit to the PnBMA MQ spectrum shown in Figure 1b yields 16-correlated ^{19}F nuclei (eq 1), indicating salt clustering. In contrast, for the PMMA film, only a small amount of two-quantum (2Q) coherence is observed in Figure 1c, indicating that the majority of the salt is dispersed. The physical interpretation of this data will be discussed in further detail later in this section, but comparing these two film shows that MQ-NMR is sensitive to the molecular-scale salt concentration rather than to the average concentration of the salt in the polymer matrix.

The multiple-quantum intensity spectrum for Ph_3SAsF_6 at room temperature for a series of preparation times, between 60 and 1380 μs, in 60-μs increments, is shown in Figure 2a. At each τ, the sum of the positive, nonzero MQ

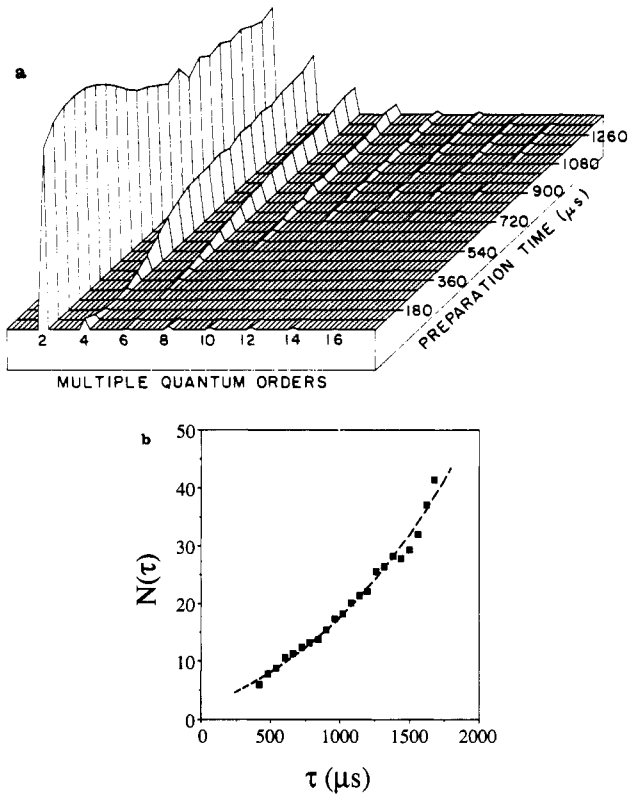

Figure 2. (a) MQ-NMR spectrum of the 98% pure photoactive salt, Ph_3SAsF_6, at room temperature showing the normalized intensities, $I(n,\tau)$, for positive, even-order, n-quantum coherences (left to right) as the preparation time, τ, is incremented (front to back). Note that a significant two-quantum coherence is present at the earliest preparation time, $\tau = 60$ μs, but that an induction period of over 300 μs is required for monotonic growth of four-quantum coherence to begin. Even longer periods are required for growth of the subsequent coherences to commence, which is indicative of the longer time required to couple larger numbers of ^{19}F nuclei. Increasing τ allows ^{19}F nuclei at larger separations to participate in MQ coherences. For $\tau > 420$ μs, the Gaussian distribution of $I(n,\tau)$ defines $N(\tau)$, the effective number of correlated ^{19}F nuclei (eq 1). (b) $N(\tau)$ values obtained from spectra analogous to those in (a) at 200 K, showing the monotonic increase to >40-coupled ^{19}F as τ is increased, where the dashed line has been drawn to aid the eye.

intensities has been normalized to unity. Note that only even-order coherences are observed due to the selective excitation used. Higher orders of MQ coherence are seen as τ increases. The 2Q coherence develops first, followed by higher orders, until 12-quantum coherence gains significant intensity at the longest preparation times.

In Figure 2b, the number of effectively coupled spins, $N(\tau)$, is plotted as a function of the preparation time, for Ph_3SAsF_6 at 200 K. $N(\tau)$ is obtained from a Gaussian fit (eq 1) to the MQ intensity distribution, $I(n,\tau)$, at each incremental value of τ. The mean R^2 correlation coefficient of these fits was 0.98. The dashed line in Figure 2b through the data is drawn to aid the eye. A considerable induction time, 420 μs, is required before ≥6 spins become correlated, which is also evidenced by the lack of monotonic growth for orders with $n > 2$ during this same time period in the corresponding MQ spectrum of Figure 2a. This long induction period reflects the large interanion spacing, of approximately 7.7 Å in the photoactive salt.[21] The largest value of $N(\tau)$, reached at the longest excitation time, is >40 spins.

In Figure 3, $N(\tau)$ data for three metal–fluoride salt/PnBMA or PiBMA films are plotted in comparison to the dashed line of Figure 2b, characterizing the 98% Ph_3SAsF_6 $N(\tau)$ growth rate. Note that the induction time required

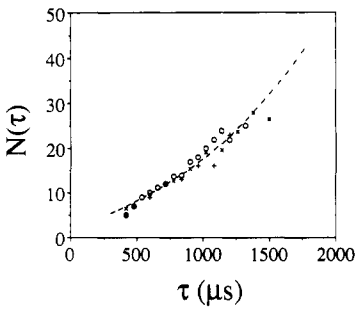

Figure 3. Similar growth of $N(\tau)$, the effective number of correlated ^{19}F, for the three photoactive salt/poly(butyl methacrylate) films: 1% Ph_3SAsF_6/PnBMA (○), 1% Ph_3SAsF_6/PiBMA (×), and 10% Ph_3SSbF_6/PnBMA (+). The difference between neither the isobutyl and n-butyl polymer side chains nor Sb and As in the photoactive salt anion effects $N(\tau)$. In fact, the MQ data of all three samples follow that for 98% pure salt (dashed curve) taken from Figure 1b, suggesting that the ionic spacings within the aggregates in the film are the same as those in the bulk salt.

Table II
Measured Glass Transition Temperature of Polymer Films

salt/polymer film	M_w	T_g, °C
PnBMA	102 000	26[a]
PMMA	70 500	108[a]
10% Ph_3SSbF_6/PnBMA	102 000	32[a]
10% Ph_3SSbF_6/PMMA	70 500	82
20% Ph_3SSbF_6/PMMA	70 500	68

[a] From ref 5.

for coupling ≥6 spins and the growth rate of $N(\tau)$ are essentially equivalent for all three salt/polymer films, and match those of the bulk salt, in spite of the fact that the salt loadings in these films are only 1% or 10%. The equivalence of the induction periods is an indication that similar spacings between the metal–fluoride anions exist in the polymer salt aggregates and the bulk salt. In addition, both the arsenate and antimonate anions yield the same $N(\tau)$ growth curve, indicating little change in anion spacing results from the difference in the metal atom. Furthermore, since the spin correlation growth rates are approximately the same for the films and the bulk salt, the predominant level of aggregation in these films is much larger than the length scale of the MQ experimental technique. No evidence of small, finite clusters, which would result in a plateau of a $N(\tau)$ versus τ plot, is observed. Figure 3 also indicates that the practical upper bound on the determination of $N(\tau)$ is about 24 correlated spins in these films. This upper limit is notably smaller than that for the 98% Ph_3SAsF_6 salt sample and can be attributed to the smaller amount of salt, by a factor of ~10, in the NMR samples of the polymer films than in the bulk salt NMR sample. Smaller samples yield correspondingly smaller signals with poor signal to noise at shorter preparation times than larger samples.

The MQ-NMR spectroscopic and DSC analyses of the 10% Ph_3SSbF_6/PnBMA mixture are in agreement. For this sample, DSC analysis shows a 6 °C increase in the bulk polymer T_g (see Table II) in addition to a bulk salt melting point peak,[5] indicating that most of the salt exists in an aggregated form with little or no mixing with the polymer chains on a molecular level. The increase in the PnBMA T_g is attributed to a salt aggregate antiplasticization phenomenon. The quality of the fit of eq 1 to the MQ coherence intensity distribution and the continuous growth of $N(\tau)$ obtained by MQ-NMR also indicate that the salt resides predominantly in an aggregated form which has interion spacings similar to those in the bulk salt.

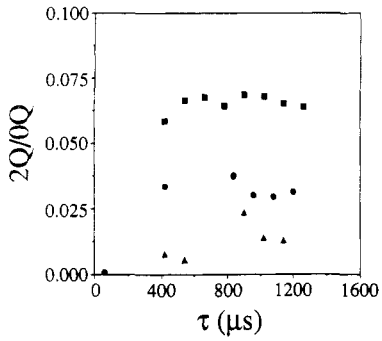

Figure 4. Two-quantum (2Q) intensity, normalized by that of the zero-quantum (0Q) coherence, as a function of preparation time, τ, for three PMMA films with various weight percents of photoactive salt; 1% Ph_3SAsF_6 (solid triangles), 10% Ph_3SSbF_6 (solid circles), and 20% Ph_3SSbF_6 (solid squares). In contrast to the PnBMA and PiBMA films (Figure 3), no MQ coherences with order >4 appear at any τ, suggesting the salt molecules are intimately mixed within the PMMA matrix and thus are isolated from one another. Note that when $\tau = 60$ μs, the 2Q in the 98% pure salt in Figure 1a is already quite intense while the 2Q has just begun to develop for the 10% salt film, suggesting that the latter has a larger interanion separation. Likewise, if the salt remains disperse, increasing the overall concentration would reduce the average interanion distance, thus increasing the 2Q/0Q ratio. Indeed, the 20% salt film has the highest 2Q/0Q ratio, while the 1% salt film has the lowest where both are <0.7, the mean 2Q/0Q ratio for the 98% pure salt, indicating the high degree of salt dispersion in the PMMA films.

The remaining films, all having a PMMA matrix with either 1% Ph_3SAsF_6, 10% Ph_3SSbF_6, or 20% Ph_3SSbF_6, have MQ coherence growth, which implies that the metal–fluoride anions are dispersed at a molecular level within the polymer. If the SbF_6^- or AsF_6^- anions were completely dispersed, such that intermolecular dipole couplings were negligible, only zero-quantum (0Q) intensity would be observed. Nonzero MQ coherences could not be created, since no significant intermolecular couplings exist and rotation averages the anion ^{19}F–^{19}F dipole couplings to zero in these materials. In fact, the 0Q intensity observed represents self-coherence from the spin state of a single nuclei, rather than the more statistically significant spin flip–flops, among groups of nuclei in a strongly dipole-coupled solid. As metal–fluoride anions are brought into ^{19}F–^{19}F interanion dipolar contact, nonzero MQ orders will begin to develop. Molecularly dispersed metal–fluoride anions in a polymeric matrix will have large interanion spacings, producing smaller ^{19}F–^{19}F dipole couplings than in pure salt crystals. Thus, the induction period for continuous spin correlation, when the MQ intensity distribution takes on a Gaussian shape (eq 1) and $N(\tau) \geq 6$, will far exceed experimentally available preparation times.

The metal–fluoride salt/PMMA films show varying amounts of 2Q coherence, depending on salt concentration. No significant n-quantum intensity greater than 2 develops for any of the PMMA films, even at the longest preparation times, indicating long MQ coherence induction times and larger interanion spacings than in the 98% Ph_3SAsF_6 salt. Thus, the salt is primarily dispersed at individual sites throughout the PMMA matrix.

In order to compare the amount of 2Q intensity for these films, the 2Q/0Q ratio has been plotted as a function of the preparation time in Figure 4. As the salt concentration is increased, the average distance between metal–fluoride anions decreases, leading to increasing 2Q coherence intensity which is observed in Figure 4. As expected, the 2Q intensity, normalized by that of 0Q, in these films is much lower than the mean 2Q/0Q ratio of 0.7 observed for nearly pure salt.

The distribution of individual salt molecules in the PMMA films is corroborated by the effect of salt loading on the polymer T_g, shown in Table II. At 10% Ph_3SSbF_6 loading, the polymer T_g of PMMA is depressed by approximately 25 °C, indicating that the salt is acting as a plasticizer and is intimately mixed with the polymer matrix. At 20% Ph_3SSbF_6 loading, the T_g is decreased by 40 °C, indicating that additional salt becomes intimately blended with the PMMA matrix, further plasticizing the polymer.

With electron microscopy, one can determine the size of visually contrasting aggregates in these amorphous films, which are quite large with respect to the length scale of MQ-NMR analysis. It is, however, impossible to make any quantitative determination of the fraction of the total salt sample which exists as the bulk salt. Aggregates on the order of 1000 Å in size have been observed in the liquid-nitrogen fracture surfaces of 10% Ph_3SSbF_6/PMMA via SEM.[5] Similar aggregate size analysis was obtained with bright-field TEM analysis of 10% Ph_3SSbF_6 in PMMA. Aggregates less than 2000 Å in size were observed with bright-field TEM measurements in a 20% Ph_3SSbF_6/PMMA film. In addition, aggregates observed via TEM were shown to be crystalline by electron diffraction. The use of TEM was hindered by the susceptibility of both the PMMA films and the photosensitive salts to electron beam damage. In the homogeneous areas of the polymer film, no contrast could be observed from the SbF_6^- anions, so that the presence of salt molecules distributed on a molecular level in the polymer matrix could not be detected.

However, the lack of continuous growth of coherences of order greater than 2 in the MQ-NMR spectra of the 10% and 20% Ph_3SSbF_6 PMMA films suggests that the predominant state of the salt within the PMMA films is a distribution of the individual molecules within the polymer chains. Since the MQ signal represents the weighted average of the distributed and aggregated environments, aggregates must represent less than 5–10% of the total salt in the film.

IR Spectroscopy. Other work involving $BiBr_3$/PMMA blends has shown that salt solubilized by interaction with the carbonyl of the polymer leads to a splitting of the IR carbonyl band.[23] However, comparison of the IR spectra of films of secondary standard PMMA (M_w = 93K) and 20% Ph_3SSbF_6/PMMA demonstrated no shift of the PMMA carbonyl peak from the addition of salt into the polymeric matrix. Comparing the 5% Ph_3SSbF_6/PnBMA film, which is opaque due to the highly clustered state of the salt in the film,[5] to the 20% Ph_3SSbF_6/PMMA film, in which the salt is primarily dispersed, indicated no shift in the IR bands which could be attributed to Ph_3SSbF_6 due to differences in molecular mixing of the salt and the polymer. The weak sulfonium salt/polymer plasticizer interaction studied here does not appear to involve the type of electron transfer between interacting chemical functional groups that would lead to shifts in the IR spectra.

Summary

The use of ^{19}F MQ-NMR for observing phase segregation in photosensitive sulfonium metal–fluoride salt/polymer films on a 10–20-Å scale has been demonstrated and compared to the more established analysis techniques of IR spectroscopy, DSC, and electron microscopy. Integrating the results of all these characterization techniques leads to the conclusion that the majority of the photoactive salt in the nonpolar butyl methacrylate polymer

films studied here, which have 1 or 10% w/w salt, exists as aggregates >20 Å in dimension. In some cases, the aggregates are larger than 1 μm in size. In addition, these aggregates are crystalline with interion spacings similar to that of the bulk salt. Films made with 10–20% w/w photoactive salt in PMMA also contain large aggregates. However, ^{19}F MQ-NMR indicates that the majority of the metal–fluoride salt in these films is intimately mixed as individual molecules within the PMMA matrix. Assuming resist sensitivity increases with the degree of salt dispersion, large salt aggregates observed by electron microscopy do not necessarily significantly decrease sensitivity if they account for only a small fraction of the total salt content.

Acknowledgment. This work has been supported by National Science Foundation Grant No. CTS-9057119. We kindly thank Dr. Robert Allen of IBM, Almaden Research Center, for supplying the Ph_3SSbF_6/polymer films studied in this work. We also thank Steve Spiegelberg and Dave Rein for assistance with TEM sample preparation, Randy Saunders for assistance with DSC, and Dr. Ananth Annapragada for IR analysis and interpretation.

References and Notes

(1) Reck, B.; Allen, R. D.; Twieg, R. J.; Willson, C. G.; Matuszczak, S.; Stover, H. D. H.; Li, N. H.; Frechet, J. M. J. *Polym. Eng. Sci.* **1989**, *29*, 960.
(2) Ito, H. *Proc. SPIE–Adv. Resist Technol. Process. V* **1988**, *920*, 33.
(3) O'Brien, M. J.; Crivello, J. V. *Proc. SPIE–Adv. Resist Technol. Process. V* **1988**, *920*, 42.
(4) Tarascon, R. G.; Reichmanis, E.; Houlihan, F.; Shugard, A.; Thompson, L. F. *Polym. Eng. Sci.* **1989**, *29*, 850.
(5) Allen, R. D.; Schaedeli, U.; McKean, D.; MacDonald, S. *Polym. Mater. Sci. Eng.* **1989**, *61*, 185.
(6) McKean, D. R.; Schaedeli, U.; Kasai, P. H.; MacDonald, S. A. *Polym. Mater. Sci. Eng.* **1989**, *61*, 81.
(7) McKean, D. R.; Schaedeli, U.; MacDonald, S. A. *J. Polym. Sci., Polym. Chem. Ed.* **1989**, *27*, 3927.
(8) Cowie, J. M. G.; Martin, A. C. S.; Firth, A.-M. *Br. Polym. J.* **1988**, *20*, 247.
(9) Spindler, R.; Shriver, D. F. *Macromolecules* **1986**, *19*, 347.
(10) Harris, C. S.; Ratner, M. A.; Shriver, D. F. *Macromolecules* **1987**, *20*, 1778.
(11) Baum, J.; Gleason, K. K.; Pines, A.; Garroway, A. N.; Reimer, J. A. *Phys. Rev. Lett.* **1986**, *56*, 1377.
(12) Petrich, M. A.; Gleason, K. K.; Reimer, J. A. *Phys. Rev. B* **1987**, *36*, 9722.
(13) Ryoo, R.; Liu, S.-B.; de Menorval, L. C.; Takegoshi, K.; Chmelka, B.; Trecoske, M.; Pines, A. *J. Phys. Chem.* **1987**, *91*, 6575.
(14) Chmelka, B.; Pearson, J. G.; Liu, S. B.; Ryoo, R.; de Menorval, L. C.; Pines, A. *J. Phys. Chem.* **1991**, *95*, 303.
(15) Wang, P.-K.; Slichter, C. P.; Sinfelt, J. H. *Phys. Rev. Lett.* **1984**, *53*, 82.
(16) Yen, Y.-S.; Pines, A. *J. Chem. Phys.* **1983**, *78*, 3579.
(17) Baum, J.; Munowitz, M.; Garroway, A. N.; Pines, A. *J. Chem. Phys.* **1985**, *83*, 2015.
(18) Baum, J.; Pines, A. *J. Am. Chem. Soc.* **1986**, *108*, 7447.
(19) Munowitz, M. *Coherence and NMR*; Wiley: New York, 1988; Chapter 6.
(20) Andrew, E. R.; Farnell, L. F.; Gledhill, T. D. *Phys. Rev. Lett.* **1967**, *19*, 6.
(21) Scruggs, B. E.; Gleason, K. K. *J. Magn. Reson.*, in press.
(22) Andrew, E. R.; Firth, M.; Jasinski, A.; Randall, P. J. *Phys. Lett.* **1970**, *31*, 446.
(23) Smid, J.; Cabasso, I.; Rawls, H. R.; Obligin, A.; Delaviz, Y.; Sahni, S. K.; Zhang, Z.-X. *Makromol. Chem., Rapid Commun.* **1987**, 543.

Registry No. PMMA, 9011-14-7; PnBMA, 9003-63-8; PiBMA, 9011-15-8; Ph_3SSbF_6, 57840-38-7; Ph_3SAsF_6, 57900-42-2.